

The VST ATLAS Quasar Survey II: Halo mass profiles of galaxies, LRGs and galaxy clusters via quasar and CMB lensing

Alice M. Eltvedt,¹★ T. Shanks,¹† N. Metcalfe,¹ B. Ansarinejad,² L.F. Barrientos,³
D.N.A. Murphy^{3,4} and D.M. Alexander¹

¹Centre for Extragalactic Astronomy, Department of Physics, Durham University, South Road, Durham, DH1 3LE, UK

²School of Physics, University of Melbourne, Parkville, VIC 3010, Australia

³Instituto de Astrofísica, Facultad de Física, Pontificia Universidad Católica de Chile, Santiago, Chile

⁴Institute of Astronomy, University of Cambridge, Madingley Road, Cambridge CB3 0HA, UK

Accepted XXX. Received YYY; in original form ZZZ

ABSTRACT

We cross-correlate a low-contamination subset of the VST ATLAS $g < 22.5$ quasar catalogue with $g < 21.5$ galaxy clusters, $r < 21$ galaxies and $r < 19.5$ Luminous Red Galaxies (LRGs) to probe their halo mass profiles via quasar magnification bias caused by weak lensing. In the case of galaxy clusters we find that at small scales their mass profiles are well fitted by Navarro, Frenk and White (NFW) models with masses within the expected range. For the galaxies, we find consistency with previous SDSS-based results for the galaxy-quasar cross-correlation and the galaxy auto-correlation functions. Disagreement as to whether the cross-correlation results are in tension with Λ CDM appears due to different assumptions as to whether galaxies trace mass. We conclude that halo occupation distribution (HOD) models fit the galaxy - quasar lensing results better than models where galaxies trace the mass. We further test the cluster and galaxy HOD models in the 2-halo range using the *Planck* Cosmic Microwave Background (CMB) lensing map, finding that the cross-correlation with both the poorest clusters and the galaxies may be marginally over-predicted by the above HOD models. Finally, we measure the magnification bias of LRGs using both quasar and CMB lensing and find that the observed quasar lensing amplitude may be $\approx 2\times$ too high and, on larger scales, the CMB lensing amplitude may be too low to be explained by a standard LRG HOD model.

Key words: quasars: general - galaxies: general - galaxies: clusters: general - dark matter

1 INTRODUCTION

The detection of the accelerated expansion of the universe (e.g. Riess et al. 1998; Perlmutter et al. 1999) as well as the existence of dark matter (Zwicky 1933; Rubin et al. 1977), as necessitated by the currently accepted Λ Cold Dark Matter (Λ CDM) model of the universe, has made the undisputed determination and understanding of these phenomena a main goal of modern astrophysics. The existence of dark energy is one possibility to explain the accelerated expansion of our universe within the framework of Einstein's theory of general relativity (e.g. Ratra & Peebles 1988) and dark matter is needed to explain observations of the clustering of structures (e.g. Peebles 1980). In terms of understanding the nature of dark matter, gravitational lensing analyses are clearly of prime interest (e.g. Narayan & Nityananda 1985; Kaiser & Squires 1993; Kaiser 1998; Myers et al. 2003).

The lensing magnification of background objects by large scale structures can also provide constraints on the cosmological parameters, especially the matter density of the universe (Ω_M) and the "clumpiness" (σ_8). Galaxy-quasar cross-correlation studies have been conducted since Seldner & Peebles (1979) detected a possible quasar excess around Lick catalogue galaxies (see also Boyle et al. 1988). More recently, works by Myers et al. (2003), Myers et al. (2005) and Mountrichas & Shanks (2007) have used background 2QZ (Croom et al. 2005) quasars to detect the effect of galaxy and galaxy cluster lensing and Scranton et al. (2005) have performed such lensing analyses using photo- z selected quasars from the Sloan Digital Sky Survey (SDSS). Myers et al. (2003) and Mountrichas & Shanks (2007) found a higher than expected amplitude of lensing magnification bias based on simple $\Omega_m = 0.3$ models that assumed galaxies traced the mass, and suggested there may be inconsistency with the standard Λ CDM model. However, Scranton et al. (2005) argued conversely that their SDSS results were compatible with the standard Λ CDM model. Ménard et al. (2010) confirmed these findings on the full SDSS imaging catalogue (while also detecting

★ E-mail: aeltvedt@alumni.princeton.edu

† E-mail: tom.shanks@durham.ac.uk

a sub-dominant contribution from galactic dust absorption to the cross-correlation functions). Here, we perform a weak gravitational lensing analysis through a cross-correlation of background quasars and foreground galaxies and galaxy clusters using the VST ATLAS Quasar Catalogue (see [Eltvedt et al. 2023](#) hereafter [Paper I](#)) to provide independent new data to further address the reasons for this apparent discrepancy.

The lensing mentioned above is defined as the gravitational deflection of photons around large masses, which causes a magnification of background sources (e.g. [Narayan 1989](#)). This "magnification bias" causes the background objects to appear brighter than they actually are while reducing the apparent solid angle behind the foreground objects, causing an increase in QSO density at bright QSO magnitudes where the slope of their number count is steeper and a decrease at fainter magnitudes where their number counts are flatter. Here we present our results, their interpretation and any implications for the cosmological model. We show that an anti-correlation is detected at faint quasar magnitudes and a positive correlation at detected at bright magnitudes as predicted by lensing. Through this cross-correlation we will be able to test (HOD) models and their assumed mass profiles over a wide range of halo masses. We shall further apply these quasar lensing analyses to galaxy cluster and LRG samples.

As an independent alternative to quasar lensing we shall also exploit CMB lensing (e.g. [Blanchard & Schneider 1987](#); [Seljak 1996](#)) by cross-correlating our ATLAS galaxy cluster, galaxy and LRG catalogues with the lensing maps of the CMB supplied by [Planck Collaboration et al. \(2018\)](#) to measure their halo profiles and fit HODs as above. Here we shall follow e.g. [Blanchard & Schneider \(1987\)](#); [Seljak \(1996\)](#) and then more recently e.g. [Krolewski et al. \(2020, 2021\)](#). We note that the resolution of the *Planck* lensing map is $\approx 6'$, giving information extending to larger angular scales than quasar lensing, while still allowing us to make direct comparisons between these two at intermediate scales in the 1-2 halo regime at $\approx 1h^{-1}$ Mpc. [Krolewski et al. \(2020, 2021\)](#) measure LRG-CMB lensing by using unWISE W1 and W2 bands ([Schlafly et al. 2019](#)) to select samples of LRGs at $z = 0.6, 1, 1, 1.4$ to produce cross-power spectra with the *Planck* lensing maps. Their main interest is to measure cosmological parameters and so they confine their studies to large scales, $60' - 900'$, whereas we complement the CMB-lensing with the small-scale QSO lensing to estimate halo mass profiles out to scales of $\approx 0.3 - 60'$, corresponding to $\approx 0.1 - 10h^{-1}$ Mpc at our LRG average redshift of $z \approx 0.26$. In [Eltvedt et al. \(2024\)](#) (hereafter [Paper 3](#)) we shall also use CMB lensing to measure the halo mass profiles of our $z \approx 1.7$ QSOs themselves, following in particular the work of [Geach et al. \(2019\)](#); [Han et al. \(2019\)](#); [Petter et al. \(2022, 2023\)](#).

The outline of this paper is as follows. Section 3 and 4 describes the cross-correlation of ATLAS selected foreground galaxy clusters and galaxies respectively with our quasar catalogue and the *Planck* CMB lensing map. We introduce HOD models in Section 5 and fit these to the quasar+CMB lensing results for the galaxy clusters and the galaxies, and also the galaxy autocorrelation function. To address the possibility that the 1-halo term is less well fitted to the galaxy cross-correlations, in Section 6 we also perform quasar and CMB lensing cross-correlations of foreground LRGs and fit HOD models that are also tested against the LRG auto-correlation function. We discuss our results in Section 7. Throughout, we assume a standard, spatially flat, cosmology with $\Omega_m = 0.3$ and a Hubble constant assumed to be $100 h \text{ km s}^{-1} \text{ Mpc}^{-1}$, with $h=0.7$ unless otherwise stated.

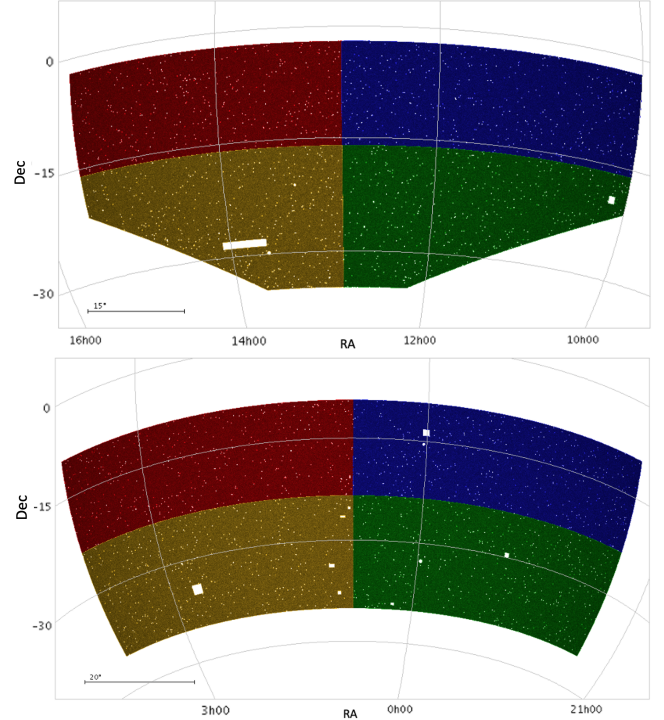


Figure 1. Maps of our random catalogue in the NGC (upper panel) and SGC (lower panel), covering the same areas as our quasar candidate catalogue. The catalogues are split into 8 approximately equal area regions to calculate errors from field-to-field variations. We have masked out Tycho stars, globular clusters, nearby dwarf galaxies and areas that are underdense due to poor observing conditions. These are left as white areas in the maps.

2 DATA CATALOGUES

2.1 Quasar Sample

The VST-ATLAS quasar catalogue described in [Paper I](#) has a certain amount of stellar and galaxy contamination, an inevitable consequence of requiring high quasar completeness. To perform these weak lensing analyses we use a more conservative, point-source only selection of our quasar catalogue to reduce galaxy contamination as well as possible overlap in the galaxy and quasar catalogues. We use the quasar candidate catalogue with the $ugri + giW1W2$ cuts described in Section 4 of [Paper I](#). We then further restrict this point-source candidate selection to $17 < g < 22$.

Following an analysis of preliminary spectroscopically confirmed QSOs, we also restrict this sample to $-0.25 < (g - r) < 0.4$, $(u - g) < 0.55$, $(r - W1) < 5$, and require $(W1 - W2) > 0.4$, again to reduce the possibility of galaxy contamination in our sample. Of this more conservative selection, we only consider quasar candidates with photometric redshifts $z > 1$ to prevent overlap in real space of quasar and galaxy samples, using results from the ANNz2 photometric redshift estimation. We also mask areas around Tycho stars to $V_T < 12.5$ following the method of [Ansarinejad et al. \(2023\)](#). Also masked are globular clusters and dwarf galaxies as well as a few areas with poor photometry. These selections result in a total of 204264 objects giving us a quasar candidate sky density of 44 deg^{-2} . The QSO distribution can be seen in Fig. 2 of [Paper 3](#) and the QSO (and galaxy) masked random catalogue is shown in Fig. 1 (see Section 3.1).

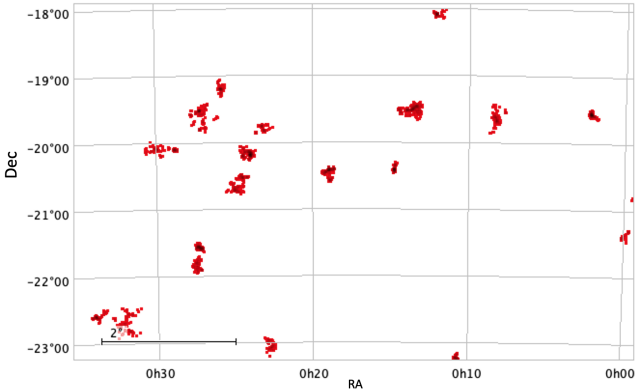


Figure 2. Sky map of defined $n \geq 40$ galaxy clusters in a section of the SGC with each point corresponding to a galaxy.

2.2 Galaxy Cluster Sample

We use the VST ATLAS Southern Galaxy Cluster Catalogue (Ansarinejad et al. 2023) to perform the angular cross-correlations between foreground galaxy clusters and background quasars. The galaxy groups and clusters in this catalogue were selected using VST ATLAS optical photometry in the *griz* bands using the ORCA cluster detection algorithm. The ORCA cluster detection algorithm (Murphy et al. 2012) finds similarities in galaxy colours and regions with a high projected surface density and then uses the friends-of-friends technique to determine galaxy clusters and groups. The selection criteria are described in full by Ansarinejad et al. (2023). This cluster catalogue overlaps the full $\sim 4700 \text{ deg}^2$ area of our VST-ATLAS quasar survey to a depth of $r_{Kron} < 21$.

We introduce the same Tycho stars and globular cluster mask as in our QSO catalogue. This galaxy cluster catalogue is then divided into clusters with 5 or more members ($n > 5$) and clusters with 40 or more members ($n > 40$). The resulting $n \geq 5$ catalogue has $N_g = 386268$ galaxies, with a galaxy cluster member sky density of 82.18 deg^{-2} and a cluster sky density of 6.54 deg^{-2} . The $n \geq 40$ catalogue has $N_g = 60210$ galaxies, with a galaxy cluster member sky density of 12.81 deg^{-2} and a cluster sky density of 0.19 deg^{-2} .

Fig. 2 shows a patch of sky in the SGC from our $n \geq 40$ galaxy group sample. The cross-correlations between the galaxy cluster and quasar catalogues are performed between quasars and individual members of each galaxy cluster rather than the center of the clusters. Therefore, the larger clusters are weighted more heavily.

2.3 Galaxy Sample

To perform the cross-correlation analyses of our quasar candidate catalogue and individual galaxies, we also generate galaxy catalogues from the VST ATLAS data using the same star/galaxy separation as for our QSO sample. To provide an accurate comparison to the work done on SDSS data by Scranton et al. (2005), we require the galaxies to have detections to $r_{sdss} < 21$, using a 0.15 mag offset to convert from ATLAS Kron r to the total r -band SDSS magnitudes, ie $r_{sdss} = r_{Kron} - 0.15$, as suggested by previous authors (e.g. Kron 1980; Metcalfe et al. 1991; Shanks et al. 2015).¹

¹ From this point, we shall refer to r_{sdss} as r_{Kron} .

We use the same Tycho stars and globular cluster mask for all of our catalogues.

2.4 Luminous Red Galaxy Sample

We perform cross correlation with LRGs to test halo occupation models in Section 6. To do this, we create a catalogue of LRGs based on the "Cut 1" $z < 0.4$ selection shown in Figure 3 of Eisenstein et al. (2001), who get an LRG sky density of 14.3 deg^{-2} . Applying their selections on our galaxy catalogue as described in 2.3, we get a sample with a sky density of 9.3 deg^{-2} . As this is lower than the 14.3 deg^{-2} sky density, we adjust the selection slightly from $r_{KRON} < 19.2$ and $r_{KRON} < 12.38 + 2.33 * (g - r) + 4 * (r - i)$ to $r_{KRON} < 19.5$ and $r_{KRON} < 12.68 + 2.33 * (g - r) + 4 * (r - i)$ to increase the density of LRGs we are getting to 16 deg^{-2} , which is as close to 14.3 deg^{-2} as can be achieved to 0.1 mag accuracy in the magnitude limit.

2.5 Star Control Sample

We create a subset of stars to check the signal of our cross-correlations between galaxy clusters and quasars, galaxies and quasars, and finally LRGs and quasars. We select stars away from the W1 limit by selecting stars in the same $r - W1$ range as the QSOs (i.e. $3 < r - W1 < 5$ and $1 < g - r < 1.4$, see Fig. 7 of Eltvedt et al. (2023)), as we noticed that stars were being lost due to potential systematic effects, such as sky subtraction, near the W1 limit. We also go to the brighter limit of $g < 21$, than the $g < 22$ limit of our VST ATLAS catalogue to decrease potential contamination, creating a control sample that is as well positioned as possible to check our work.

Previously, when we selected star control samples in the ranges $1 < r - W1 < 3$ and $0.3 < g - r < 1$ i.e. including fainter objects in W1 than existed in the QSO sample, we found anomalies where cross-correlation of galaxies and stars showed unexpected anti-correlation. This anti-correlation appeared to increase with galaxy apparent brightness. We also found that this anti-correlation was more evident in star samples that relied on stars selected at the faintest W1 and W2 NEO7 magnitudes. The effect was reduced, but still not eliminated, when DECALS DR10 "forced" W1 and W2 photometry was used instead of NEO7. We hypothesize that there may be a sky subtraction bias in W1 in the vicinity of a bright galaxy where the sky brightness may be over-estimated. The effect was particularly evident in stars selected in $grW1$ to lie at $r - W1 < 2$. This selection is otherwise optimal in avoiding galaxy contamination (see Paper I) but since our QSO samples reach $g \approx r \sim 22$ this means the equivalent star sample reaches $W1 \sim 21$ compared to a NEO7 limit of $W1 \sim 20$ so these samples suffer high incompleteness and will be more prone to the sky subtraction issue postulated above. When a control star sample with an $r - W1$ distribution more similar to the QSOs was used (i.e. $1 < g - r < 1.4$ and $3 < r - W1 < 5$), this anti-correlation reduced significantly. We considered the possibility that galaxy contamination in this star sample might also contribute to this reduction. However, simple $g < 22.5$ star samples with no colour selection also gave no evidence of anti-correlation so we concluded that the star-galaxy anti-correlation is only serious in star samples too close to the W1 limit. In this case the effect on our QSO samples will be small. But we shall show the star-galaxy correlation results alongside the quasar-galaxy correlation results so that the size of any possible systematic effect can be judged.

2.6 CMB Lensing Data

We use the 2018 release of the Planck lensing convergence baseline map, using the CMB-only minimum variance estimates of the lensing signal to scales of $l = 4096$ (Planck Collaboration et al. 2018), to perform cross-correlations with our galaxy, galaxy cluster, and LRG samples. Small angular scales correspond to a high l value as $\theta \sim \frac{180 \text{ deg}}{l}$. The Healpix a_{lm} are first smoothed with a Gaussian filter with a FWHM of 15 arcmin. We then convert this baseline Minimum Variance lensing map from the stored convergence spherical harmonics a_{lm} to a Healpix map (as done by Geach et al. 2019) with $n_{\text{side}} = 2048$ and an $l_{\text{max}} = 4096$. This then gives us a list of RA and Dec coordinates of the Healpix pixel centers. We apply the lensing mask provided by the Planck Collaboration et al. (2018) to the CMB data and select two areas that overlap our $\sim 4700 \text{ deg}^2$ QSO sample.

2.7 Possible systematic effects

Contamination of the QSO sample by stars or galaxies will show different effects on our cross-correlation results. Star contamination will dilute bright and faint cross-correlations by the fraction of stars in the QSO sample. However, the g_{rW1} cut we make is very efficient at removing stars at the $g < 22$ magnitude range of our QSO sample. So the main QSO contaminant is likely to be galaxies in the same redshift range as the $r < 21$ galaxy sample and this will reduce galaxy QSO anti-correlation at faint magnitudes while increasing galaxy-QSO cross-correlation at bright QSO magnitudes. However, the restricted version of our quasar sample which we are using reduces this contamination (see Section 2.1). We shall see that the level of agreement between the positive and negative cross-correlations seen at bright and faint QSO magnitudes with a lensing model can be taken as confirming this low level of galaxy contamination.

A similar argument applies to any dust obscuration associated with the foreground galaxy population, since this would increase the anti-correlation at faint QSO magnitudes while decreasing the positive signal at bright magnitudes, producing disagreement with the lensing model. Ménard et al. (2011) did find evidence for dust effects in the SDSS galaxy-QSO cross-correlations but they were highly sub-dominant with respect to the lensing effect. We tested limiting our QSO sample in the W1 band and compared the galaxy-QSO cross-correlations to those found in the g -limited QSO samples and again found little difference between the two, implying that lensing dominates our cross-correlation results.

The other major systematic was the possible sky subtraction issue in W1, W2 in the vicinity of bright galaxies. This evidenced itself in a strong anti-correlation between bright galaxies and stars. However, the effect reduced when the star control sample was selected to have r -W1 colours more similar to the QSOs (see Section 2.5) and we show these galaxy-star cross-correlations alongside the galaxy-QSO versions in Figs. 7 and 10, for comparison purposes.

3 QSO - GALAXY CLUSTER LENSING

3.1 Cross-Correlation Method

We use the data samples described in Section 2 to make a weak gravitational lensing analysis via a cross-correlation of background quasars and foreground galaxies and galaxy clusters. Following

Limber's equation (Limber 1953), we can express the 3-D correlation function (and power spectrum) as 2-D angular correlations. To calculate the angular cross-correlation, we need random data sets with the same input parameters as our quasar + galaxy/galaxy cluster samples. Therefore, we generate catalogues of uniformly distributed random points covering the same area as our survey with typically > 10 times as many sources as the observable data sets. These random catalogues are then also masked in the same manner as our data catalogues (see Fig. 1).

We use the publicly available Correlation Utilities and Two-point Estimates (CUTE) code (Alonso 2012) to determine the angular cross-correlation of our samples. CUTE calculates the cross-correlation by using the normalized Landy-Szalay estimator for a two-point correlation function, defined as:

$$\omega_{GQ}(\theta) = \frac{D_G D_Q - D_G R_Q - R_G D_Q - R_G R_Q}{R_G R_Q}, \quad (1)$$

We check the output generated by the Landy-Szalay estimator by manually checking the $D_G D_Q$, $D_G R_Q$, $R_G D_Q$, and $R_G R_Q$ outputs which we need to calculate the angular cross-correlation. Here $D_G D_Q$ denotes the number of data-point pairs drawn from the galaxy sample and quasar sample with separation θ . For $D_G R_Q$ the quasar sample is replaced with the sample of randomly distributed quasar points with the same angular selection function as the data. Similarly, for $R_G D_Q$ the galaxy sample is replaced with our random galaxy sample. The $R_G R_Q$ output is the number of data-point pairs drawn from the two random quasar and galaxy samples.

To generate error estimates from field-field variations, we divide the quasar and galaxy samples into $N_s = 8$ similarly sized $\approx 600 \text{ deg}^2$ regions, 4 in the NGC and 4 in the SGC. These fields are shown in Fig. 1. Then we estimate the standard errors of the cross-correlation by using the field-field error:

$$\sigma_{\bar{\omega}}(\theta) = \frac{\sigma_{N_s-1}}{\sqrt{N_s}} = \sqrt{\frac{\sum (\omega_i(\theta) - \bar{\omega}_i(\theta))^2}{N_s^2 - N_s}}, \quad (2)$$

where the sum is over $i = 1, N_s$.

3.2 Quasar-Galaxy Cluster Lensing SIS Model

The lensing of the background objects depends on the mass profiles of the foreground objects. For galaxy clusters, we initially assume the simplest mass profile of a singular isothermal sphere (SIS). The deflection angle of sources by such foreground lenses is given by:

$$\alpha = \frac{4GM(< b)}{bc^2} = \frac{D_s}{D_{ls}}(\theta - \theta_q), \quad (3)$$

(e.g. Myers et al. 2003) where b is the impact parameter, $M(< b)$ is the mass contained within the radius of the lens, D_s is the angular diameter distance from the observer to the source, D_{ls} is the angular diameter distance from the source to the lens, θ is the angle from the observer's line of sight to the image, and θ_q is the angle from the observer's line of sight to the source quasar.

We see an increase in apparent brightness/magnitude of the background object as the surface brightness of the object is conserved, but spread across a larger surface area. Therefore the flux received from the object is increased. The magnification, A , of the object due to a foreground lens can be described as:

$$A = \left| \frac{\theta}{\theta_q} \frac{d\theta}{d\theta_q} \right| \quad (4)$$

On the assumption of lensing by a SIS, the mass surface density is:

$$\Sigma_{SIS} = \frac{\sigma^2}{2Gr} \quad (5)$$

where σ is the velocity dispersion of the SIS and the density goes as $\rho(r) = \frac{\sigma^2}{2\pi Gr^2}$. This can be integrated over a radius of $r = 0$ to $r = b$ and combined with Eq. 3 to give the amplification due to a SIS of a background source at radius θ :

$$A = \left| \frac{\theta}{\theta - 4\pi \left(\frac{D_{LS}}{D_s}\right) \left(\frac{\sigma}{c}\right)^2} \right| \quad (6)$$

This amplification factor can also be described as the ratio of the lensed flux and the unlensed flux (Croom 1997). As the amplification affects the relative distribution of background and foreground objects, we can relate the angular cross-correlation to the amplification factor through:

$$\omega(\theta) = A^{2.5\alpha-1} - 1 \quad (7)$$

where α is the slope of the cumulative source number count, $d\log(N)/dm$. Zero correlation is predicted at $\alpha = 0.4$ with an anti-correlation at $\alpha < 0.4$, and a positive correlation at $\alpha > 0.4$.

In our model, we use the flat Λ CDM cosmology, with $\Omega_M = 0.3$ and $\Omega_\Lambda = 0.7$. We assume an average foreground galaxy sample and galaxy cluster redshift of $z = 0.15$ and an average quasar sample redshift of $z = 1.5$. This gives us an angular diameter distance of the quasar sample $D_S = 1780$ Mpc and $D_{LS} = 1235$ Mpc. We also use a lensing coefficient of $2.5\alpha - 1 = -0.37$ for the faint QSOs with $20 < g < 21$ and $2.5\alpha - 1 = 0.95$ for the bright QSOs with $17 < g < 19$ taking these and other values from Table 1 of Scranton et al. (2005) for consistency with their assumptions.

3.3 Quasar-Galaxy Cluster Lensing NFW Model

Similar to modelling the cluster lensing via SIS we next model the clusters using an (Navarro, Frenk & White 1996) NFW model. We follow this route here because the HOD approach for clusters is less developed than for galaxies. Nevertheless, for computational convenience we use the Cosmology and Halo Model Python code (CHOMP), which is a halo modelling package written by Morrison, Scranton, and Schneider to produce the projected, lensed NFW mass profile which in 3-D takes the form:

$$\rho(r) = \frac{\rho_0}{(r/r_s)(1+r/r_s)^2}, \quad (8)$$

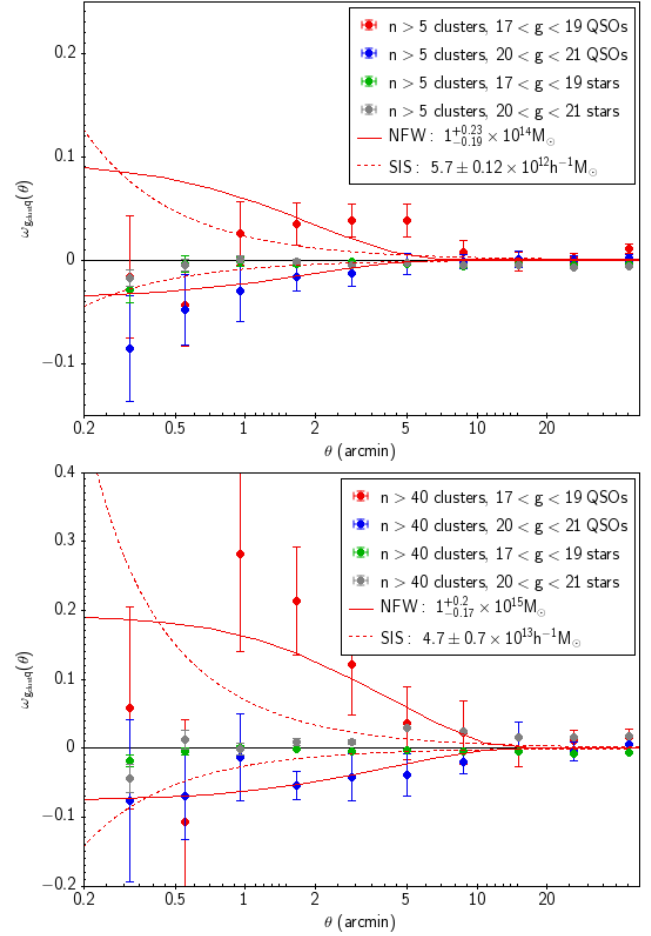


Figure 3. Results of the cross-correlation of both our bright and faint quasar candidate catalogues in the g -band and the VST ATLAS galaxy cluster catalogue for clusters comprised of $n > 5$ and $n > 40$ galaxies, using the CUTE code for angular cross-correlation. The SIS model here has a velocity dispersion of 270 km s^{-1} and 460 km s^{-1} and the HOD models are using a halo mass of 10^{14} solar masses for the $n > 5$ galaxy clusters, and a halo mass of 10^{15} solar masses for the $n > 40$ galaxy clusters. The positive models are for the bright QSO-galaxy cluster cross correlation results and the negative models are for the faint QSO-gal cluster cross correlation results.

CHOMP also assumes that halo concentration is a function of halo mass with the functional form $c(m) \approx 9(m/m^*)^{-0.13}$ taken from Bullock et al. (2001). We then compute these projected, lensed NFW mass profiles by simply isolating the NFW part of the 1-halo term produced by CHOMP. Full details of the 1- and 2-halo terms and their projection and magnification as implemented in CHOMP are given by Jain et al. (2003) and will be further summarised in Section 5.

3.4 Quasar-Galaxy Cluster Cross-Correlation Results

We perform the cross-correlation of our $n > 5$ and $n > 40$ galaxy cluster catalogues with our $17 < g < 19$ and $20 < g < 21$ quasar samples. We test the robustness of our detections by performing the cross-correlations with star samples in the same magnitude ranges. We can see in Fig. 3 a clear anti-correlation with the faint, $20 < g < 21$, quasar samples for both the $n > 5$ and $n > 40$ galaxy clusters. The cross-correlations with the faint star samples show

Table 1. Summary of results for galaxy cluster masses. w_{cq} denotes the cluster-QSO cross-correlation, shown for the SIS and NFW cases, and w_{ck} is the cluster-CMB cross-correlation. A2023 cluster masses are estimated by [Ansarinejad et al. \(2023\)](#)

Method	$n > 5$ Mass ($10^{13}h^{-1}M_{\odot}$)	$n > 5$ χ^2_{red}	$n > 40$ Mass ($10^{13}h^{-1}M_{\odot}$)	$n > 40$ χ^2_{red}
w_{cq} SIS	0.57 ± 0.12	1.8	4.7 ± 0.7	2.0
w_{cq} NFW	10.0 ± 2.1	1.6	100 ± 20	0.5
w_{ck} NFW	3.2 ± 0.7	3.2	32 ± 12	1.1
A2023	23 ± 8	–	43 ± 27	–

virtually zero correlation in comparison, making a strong argument for the reality of our detected cluster-quasar cross correlation signals at both bright and faint QSO magnitudes in Fig. 3.

We perform a χ^2 test for both the SIS model and the NFW based HOD model on the cross-correlation results in order to determine which model best describes our results in Figs. 3. To do this, we use the inverse variance weighted mean of the bright and faint QSO cross-correlation results for both the $n > 5$ and $n > 40$ galaxy cluster cases.

For the SIS model, we find that the $n > 5$ galaxy cluster - QSO cross-correlation has a best fit velocity dispersion of $\sigma = 270_{-65}^{+50} \text{ km s}^{-1}$ with a reduced χ^2 of 1.8 and the $n > 40$ galaxy cluster - QSO cross-correlation has a best fit velocity dispersion of $\sigma = 460_{-80}^{+60} \text{ km s}^{-1}$ with a reduced χ^2 of 2.0. Using the $M = \frac{2\sigma^2 r}{G}$ relation appropriate for an SIS model and taking $r = 0.17h^{-1} \text{ Mpc}$ and $r = 0.48h^{-1} \text{ Mpc}$ for $n > 5$ and $n > 40$ clusters respectively as empirically estimated from the cluster data themselves.² These velocity dispersions correspond to masses of $5.7 \times 10^{12} h^{-1} M_{\odot}$ for $n > 5$ clusters and $4.7 \times 10^{13} h^{-1} M_{\odot}$ for $n > 40$ (see Table 1).

For the NFW profiles, we similarly perform a χ^2 fit to the w_{cq} , finding that the $n > 5$ clusters are best fit by a mass of $10^{14 \pm 0.09} h^{-1} M_{\odot}$ with a reduced χ^2 of 1.6 and the $n > 40$ cluster cross-correlations are best fit by $10^{15 \pm 0.08} h^{-1} M_{\odot}$ with a reduced χ^2 of 0.5.

We conclude that the NFW is a better fit for the galaxy cluster-QSO cross-correlation as the SIS generally appears to be too steep at small scales, while the NFW is better able to fit the dampening of the signal at small scales. The implied NFW mass for $n > 40$ clusters also is more in agreement with the mass estimates of [Ansarinejad et al. \(2023\)](#), based on various calibrations of cluster membership, that gave a mean mass of our $n > 40$ galaxy clusters of $4.3 \pm 2.7 \times 10^{14} h^{-1} M_{\odot}$ (see Table 1).

3.5 Galaxy Cluster - CMB Lensing Map Cross-Correlation

Galaxy cluster-QSO cross-correlation mainly probes the 1-halo term, whereas cross-correlation of the Planck CMB lensing convergence map with the galaxy clusters only constrains the 2-halo term due to the $\approx 6'$ Planck resolution. Nevertheless, we can check if the NFW profiles found to fit our QSO-galaxy cluster cross-correlations give halo masses consistent with the CMB lensing method. We model the CMB lensing by foreground galaxy clusters using the 5-parameter HOD methodology of [Zheng & Weinberg](#)

² These cluster radii were empirically estimated from the cluster membership, assuming an $8\times$ overdensity on the sky, covering a circular area, and an average redshift of $z = 0.2$ as suggested by [Ansarinejad et al. \(2023\)](#).

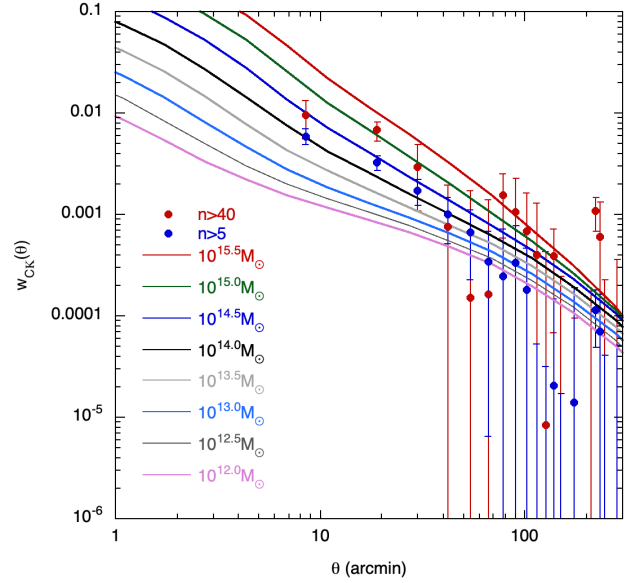


Figure 4. w_{ck} cluster-CMB cross-correlation functions for $n > 5$ and $n > 40$ clusters compared to w_{ck} predicted by supplying CHOMP with the [Zheng & Weinberg \(2007\)](#) HOD parameters of $\log(M_{min}) = 12.0, 12.5, 13, 13.5, 14, 14.5, 15$, $\log(M_0) = \log(M_{min})$, $\log(M_{1'}) = \log(M_{min}) + 1.08$, $\sigma_M = 0.4$ and $\alpha = 0.7$ with masses in solar mass units assuming $h = 0.7$. The models were integrated over the redshift range $0.01 < z < 0.36$ and $\sigma_8 = 0.8$ was assumed throughout.

(2007). We again employ the above CHOMP halo modelling package and here use it more conventionally, to make 1-halo + 2-halo predictions, with the latter dominant. We assume the following HOD parameters $\log(M_0) = \log(M_{min})$, $\log(M_{1'}) = \log(M_{min}) + 1.08$, $\sigma_M = 0.4$ and $\alpha = 0.7$ with masses in solar mass units assuming $h = 0.7$. These parameters are used for values of $\log(M_{min}) = 12.0, 12.5, 13, 13.5, 14, 14.5, 15$ to probe a similar range of masses studied previously for both the SIS and NFW QSO lensing models. We assume a flat redshift distribution between $z = 0.01$ and $z = 0.36$ as an approximation for our cluster samples (see [Ansarinejad et al. \(2023\)](#)) and a flat redshift distribution is also assumed for the CMB between $z = 1050$ and $z = 1150$.

Shown in Fig. 4, we see the result of cross-correlating the $n > 5$ and $n > 40$ galaxy clusters with the CMB lensing convergence map, along with the various HOD results. There is a potential smoothing at the smallest scales here due to the $6'$ resolution of the Planck CMB lensing convergence data. Therefore, the results in the bin at the smallest scale may be more systematically uncertain than indicated by the field-field error bars.

Performing a χ^2 fit of the models to the data we find that the cross-correlation of the $n > 5$ clusters with the CMB lensing convergence map is best fit by a HOD with $\log_{10}(M_{min}) = 13.5_{-0.11}^{+0.09}$ with a reduced χ^2 of 3.2, which is not a good fit. For cross-correlation of $n > 40$ clusters, we get a best fit model with $\log_{10}(M_{min}) = 14.5_{-0.2}^{+0.14}$ with a reduced χ^2 of 1.1, with the corresponding NFW 1-halo term from QSO lensing giving $\log(M_h) = 15$. In general, the cross-correlation of galaxy clusters with the Planck CMB lensing convergence map seem to agree with the NFW model results from QSO lensing in the previous section, although the $n > 40$ fit has a slightly lower 2-halo mass than the NFW fit for the 1-halo term. We see a more significant departure in the halo mass predictions of the SIS model with the SIS masses being $\approx 10\times$ smaller than the

NFW masses, as summarised in Table 1. The average masses of the $n > 5$ and $n > 40$ clusters as estimated by Ansarinejad et al. (2023) are also given in Table 1. We see that for $n > 40$ clusters, our NFW lensing masses bracket the estimate of Ansarinejad et al. (2023) and so are in good agreement. For $n > 5$ clusters the QSO and CMB lensing masses are a factor of $\approx 2\times$ smaller than that of Ansarinejad et al. (2023) and so the agreement is less good here.

We conclude that for the richer, $n > 40$, galaxy clusters, the NFW density profile fits significantly better than the SIS profile at the small, 1-halo, scales probed by our QSO lensing results. Generally the SIS profiles are too centrally peaked compared to the QSO lensing data. At larger scales, the CMB lensing results for these richer clusters also suggest that they are well-fitted by a HOD model with a 2-halo term based on a Λ CDM cosmology. The estimated average mass for these richer clusters, assuming NFW/ Λ CDM 1+2-halo terms, is in the range $3 \times 10^{14} - 1 \times 10^{15} h^{-1} M_{\odot}$, in good agreement with mass estimates from Ansarinejad et al. (2023) and other authors.

For the less rich $n > 5$ groups and clusters, the QSO lensing statistics are poorer and here both the 1-halo NFW and the SIS models provide acceptable fits to these data. The best-fitting NFW model implies a mass of $\approx 1 \times 10^{14} h^{-1} M_{\odot}$ for this $n > 5$ sample, a factor of $\approx 2\times$ lower than the estimate of Ansarinejad et al. (2023) but in agreement within the errors. At larger scales, the CMB lensing signal for this $n > 5$ sample is strongly detected at a level almost as high as for the $n > 40$ sample. However, in this case, a HOD model based on a Λ CDM cosmology and where the minimum halo mass was allowed to vary in the range $1 \times 10^{12} < M_{\min} < 3 \times 10^{15} h^{-1} M_{\odot}$ could not be found to fit the CMB lensing data when fitted over the full $\theta < 300'$ range. The reason for this disagreement is currently unclear but will be further investigated in the work on galaxy lensing following in Sections 4 and 5.

4 QSO-GALAXY CROSS-CORRELATION

We now turn to estimating foreground galaxy halo masses via the lensing of background QSOs and the CMB, complemented by constraints from the angular autocorrelation function of the same galaxies. For the galaxy-QSO cross-correlations, we shall first use a model where galaxies trace the mass to connect with the previous studies of, e.g. Myers et al. (2003), before dropping this assumption and fitting HOD models (such as Scranton et al. 2005; Jain et al. 2003; Zheng & Weinberg 2007 etc).

4.1 Quasar-Galaxy Cross-Correlation Model

We first use the Williams & Irwin (1998) model, as outlined by Myers et al. (2005), to describe the correlation between our quasar sample and foreground galaxies. Although Myers et al. (2005) uses a galaxy sample to $g < 20.5$, we use a galaxy sample of $r < 21$ in order to match the magnitude limit of the SDSS galaxy sample of Scranton et al. (2005). This Williams & Irwin (1998) (from here referred to as the WI model) bases predictions for w_{gq} on the auto-correlation, w_{gg} , of the galaxy sample and on the assumption that galaxies trace the mass. The lensing convergence κ is defined as:

$$\kappa = \frac{\Sigma(D_l, \theta)}{\Sigma_{cr}(D_l, D_s)}, \quad (9)$$

where D_l is again the angular diameter distance of the lens,

$\Sigma(D_l, \theta)$ is the surface mass density of the lens, and $\Sigma_{cr}(D_l, D_s)$ is the critical mass surface density, defined in Myers et al. (2005) as $\Sigma_{cr}(D_l, D_s) = \frac{c^2}{4\pi G} \frac{D_s}{D_l D_s}$.

We can estimate the effective convergence using the relation :

$$\kappa_{eff}(\theta) = \frac{3H_0^2 c}{8\pi G} \Omega_m (\delta_G - 1) \int_0^{z_{max}} \frac{(1+z)^3 \frac{dt}{dz} dz}{\Sigma_{cr}(z, z_s)}, \quad (10)$$

(see Myers et al. 2005; Williams & Irwin 1998). Here, we take $z = 1.5$ as the median redshift of our quasar sample and the galaxy sample peaks at ~ 0.2 , so we integrate to a redshift of $z_{max} = 0.3$ where the distribution drops to $\sim 20\%$. From this calculation, we find $\bar{\kappa} = 0.025$. The quasar-galaxy cross-correlation can then be modelled using the ω_{gg} and a Taylor expansion of Eq. 7. Therefore we predict the galaxy-quasar cross-correlation using:

$$\omega_{gq}(\theta) = (2.5\alpha - 1) \frac{2\bar{\kappa}}{b} \omega_{gg}(\theta), \quad (11)$$

where $\frac{\bar{\kappa}}{b} = \frac{\kappa_{eff}(\theta)}{(\delta_G - 1)}$. Here b represents the linear galaxy bias $b = \langle \delta_G - 1 \rangle / \langle \delta_M - 1 \rangle$. The r.m.s. galaxy fluctuation $\langle \delta_G \rangle$ will be estimated via ω_{gg} , here represented by a power law fit to our galaxy sample acf which gives $\omega_{gg} = 0.142\theta^{-0.70}$ in the range $\theta < 120'$, as shown in Sec. 5.

In passing, we note the excellent agreement of the ATLAS $17 < r < 21$ galaxy w_{gg} with the equivalent SDSS w_{gg} of Wang et al. (2013) also shown in Fig. 7 (a). Given this SDSS-ATLAS acf agreement extends to $\theta = 8\text{deg.}$ or $r_{com} \approx 90h^{-1}\text{Mpc}$ at the average galaxy redshift of $z \approx 0.22$, this represents a strong argument for the accuracy of these two independent results and also for the reliability of their parent datasets.

4.2 Quasar-galaxy cross-correlation results

The results of cross-correlating our ATLAS QSO catalogue in various magnitude ranges with our $17 < r < 21$ mag galaxy catalogue is shown in Fig. 5. Also shown is the HOD model from the SDSS results of Scranton et al. (2005) in blue, and the WI model described in the previous section is shown in red. At angular scales of $\theta < 5'$, we see a negative cross-correlation between ATLAS quasars and foreground galaxies at quasar g-band magnitudes of $g > 20$ whereas at brighter QSO limits we see a positive correlation. These are the same trends as seen by Scranton et al. (2005) and by Myers et al. (2003, 2005) previously and they are as expected on the basic theoretical lensing model described in Section 4.1.

To ease model comparisons between Scranton et al. (2005) and ourselves, we use the values for $\langle \alpha_{505} - 1 \rangle = (2.5\alpha - 1)^3$ listed in Table 1 and Fig. 2 of Scranton et al. (2005). Then, using our $w_{gg} = 0.142\theta^{-0.70}$ fit, with $\bar{\kappa} = 0.025$ and $(2.5\alpha - 1) = -0.37$, we see from Fig. 6 that the best fit for the galaxy bias is $b = 0.5^{+0.13}_{-0.09}$ for the ATLAS cross-correlation at $20 < g < 21$. Here, the fit based on 9(5) points in the range $\theta < 30'(4')$, yields low reduced $\chi^2 = 0.4(0.6)$. Also in this fit the covariance between the

³ Note that α_{505} refers to a flux limited power law QSO number count, $N(> f)$ in the notation of Scranton et al. (2005), whereas in our notation α refers to a magnitude limited power law number count, $N(< m)$.

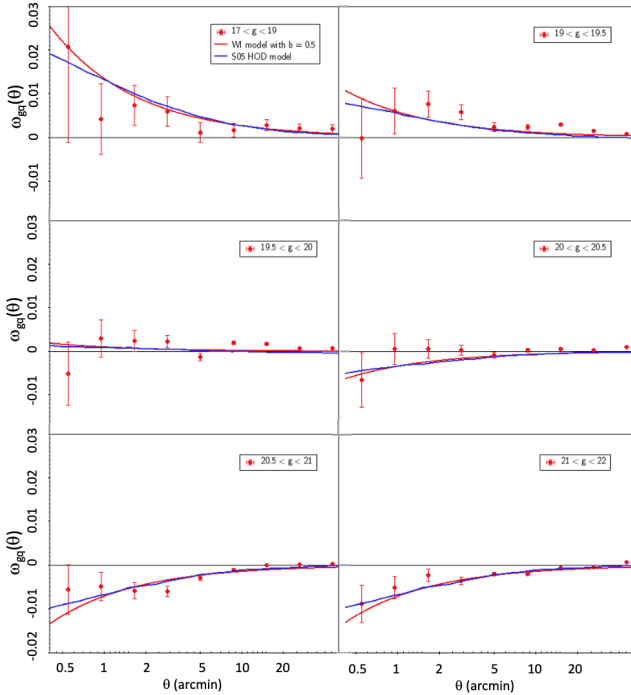


Figure 5. Cross-correlations of our quasar candidate catalogue at $17 < g < 19$, $19 < g < 19.5$, $19.5 < z < 20$, $20.5 < g < 21$, and $21 < g < 22$ and our VST ATLAS galaxy catalogue at $r < 21$, using the CUTE code for angular cross-correlation across the full sky. We also add the [Scranton et al. \(2005\)](#) HOD model for each of the quasar g -band magnitude bins. A bias value of $b = 0.5$ is consistently assumed for our WI model in red. The $\langle 2.5\alpha - 1 \rangle$ values for each QSO magnitude range for both our model and the [Scranton et al. \(2005\)](#) model are as follows: 0.95 for QSOs in the $17 < g < 19$ range, 0.41 for $19 < g < 19.5$, 0.07 for $19.5 < g < 20$, -0.24 for $20 < g < 20.5$, and -0.5 for $20.5 < g < 21$. We also assume this -0.5 value for the $21 < g < 22$ range.

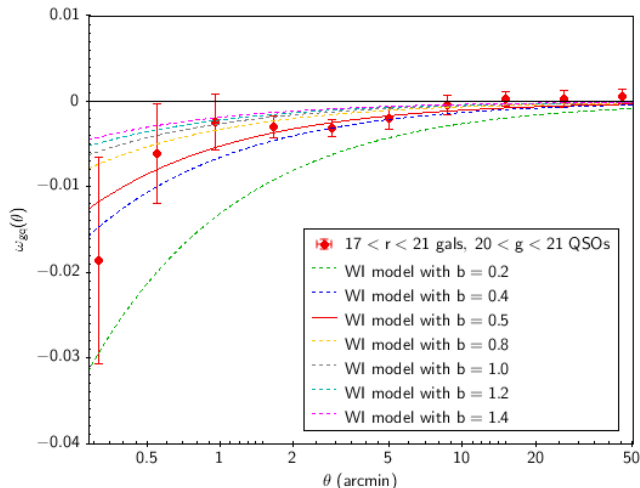


Figure 6. Our $\omega_{gg} = 0.142\theta^{-0.70}$ model fit, with $\bar{\kappa} = 0.025$ and $\langle \alpha - 1 \rangle = 0.37$, with bias values of $b = 0.2$, $b = 0.4$, $b = 0.5$, $b = 0.8$, $b = 1.0$, $b = 1.2$, and $b = 1.4$ for our cross-correlation at $20 < g < 21$.

ω_{gq} points is ignored since it is usually sub-dominant, due to the low space density of quasars ([Boyle et al. 1988](#)). As previously noted, these cross-correlation amplitudes are high as measured by the simple WI model since $b = 0.5$ corresponds to $\sigma_8 \approx 2^4$ when the usual range is $0.7 < \sigma_8 < 0.8$ (e.g. [Planck Collaboration et al. 2020](#); [Heymans et al. 2021](#)) i.e. $1.25 < b < 1.4$.⁵ Certainly, the $b = 1.25$ (i.e. $\sigma_8 \approx 0.8$) model appears to give a poor fit in Fig. 7(c), with the 5 points at $0.5' < \theta < 8'$ giving a reduced $\chi^2 = 2.60$, rejecting the model at the 5% significance level. However, dropping the assumption that galaxies trace mass may mean that models can be found that are more consistent with Λ CDM.

So as previously suggested by [Mountrichas et al. \(2009\)](#), we first conclude that there is little disagreement in terms of the observed data between SDSS and our ATLAS results and that the main disagreement is between these two models. We further conclude that the [Williams & Irwin \(1998\)](#) assumption that galaxies trace the mass is unlikely to be correct, given that would imply $b = 0.5$ i.e. $\sigma_8 = 2$ in contradiction with all observed CMB power spectra. So models that drop this assumption, like the S05 HOD model, are likely to be required. However, the S05 HOD model may still underestimate the lensing signal, particularly at small $\theta < 0.5'$ scales. So in Section 5 we shall look for a HOD model that improves the w_{gq} fit while also simultaneously fitting the w_{gg} of our $17 < r < 21$ galaxy sample.

5 HOD MODELS VIA QUASAR-GALAXY LENSING AND GALAXY-GALAXY CLUSTERING

5.1 Modelling galaxy-galaxy angular correlations

We now make a further check of the [Scranton et al. \(2005\)](#) HOD model using their publicly available code from the CHOMP GitHub site written by [Morrison, Scranton, and Schneider](#). The code follows [Jain et al. \(2003\)](#) in making predictions for both the angular auto-correlation function w_{gg} and the galaxy-mass cross-correlation function w_{gk} based on a mass power-spectrum, $P(k)$, and a HOD, with the average number of galaxies per halo of mass M being denoted by $\langle N(M) \rangle$.

First, we have assumed the simple HOD model $\langle N(M) \rangle = 1 + (M/10^{12.15})^{1.0}$ for $M > 10^{11.15} M_\odot$ (with $h = 0.7$) used by [Scranton et al. \(2005\)](#) and we use this to predict w_{gg} for the $17 < r < 21$ galaxy sample used here (see Fig. 7a). We note in passing that [Scranton et al. \(2005\)](#) did not compare their observed and predicted w_{gg} . We found that this model with $\sigma_8 = 0.8$ over-predicted w_{gg} at $\theta < 5'$ and under-predicted it at larger, $\theta > 5'$, scales. This under-prediction of the 2-halo term relative to the 1-halo term seems a common characteristic of HOD models. Essentially, the observed w_{gg} seems to show a more exact power-law behaviour than the HOD models. [Mead & Verde \(2021\)](#) and references therein suggest that halo models generally underpredict the Λ CDM power-spectrum in the region between the 1- and 2-halo terms. Indeed, [Peebles \(1974, 1980\)](#) expressed doubts as to whether a preferred (halo) scale could ever be produced by the smooth $1/r^2$ power-law behaviour of Newtonian gravity.

⁴ If we assume $\sigma_{gg,8} \approx 1$ then $b = 1.25$ corresponds to $\sigma_8 = \sigma_{gg,8}/b \approx 0.8$ whereas $b = 0.5$ corresponds to $\sigma_8 \approx 2$.

⁵ We note that assuming $\Omega_m = 1$ in eq 10 would also increase the cross-correlation amplitude and imply a fitted bias value of $b \approx 1.7$. Although this value is close to the expected $b = 2$ for this cosmology, this $\Omega_m = 1$ model is excluded by CMB + H_0 constraints and so we restrict our attention here to the standard cosmological model with $\Omega_m = 0.3$.

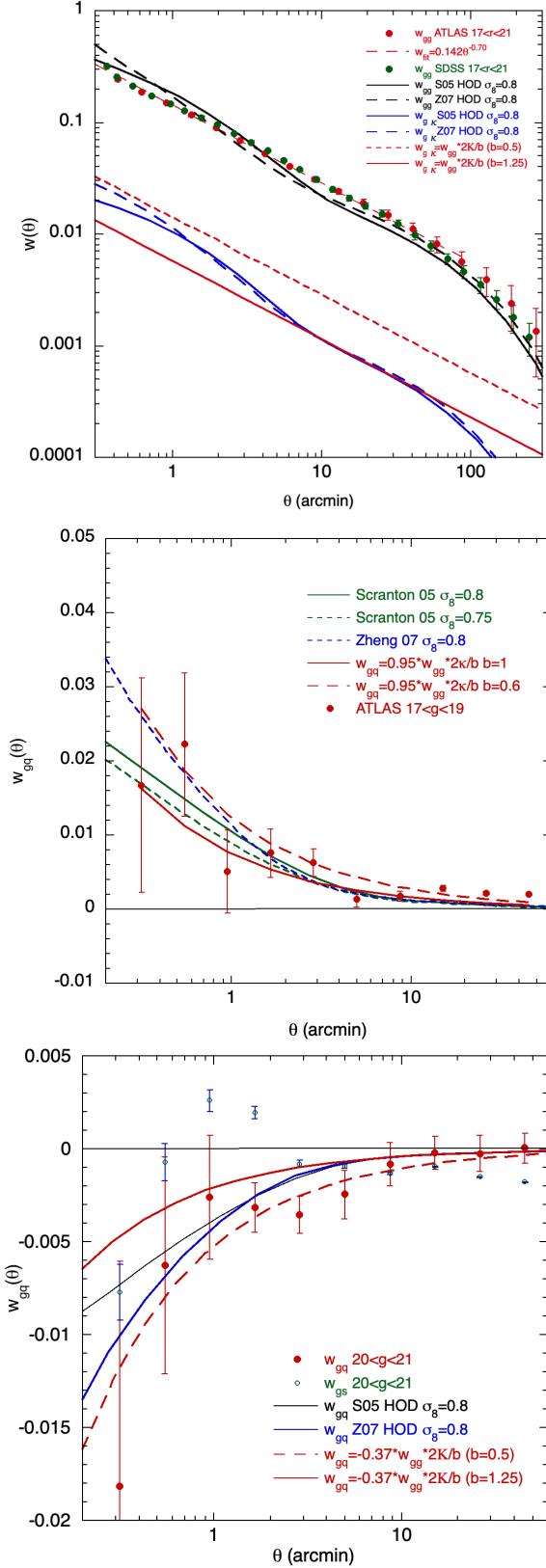


Figure 7. (a) w_{gg} and w_{gk} auto- and cross-correlation functions predicted by the HOD models of Scranton et al. (2005) and Zheng, Coil & Zehavi (2007) (with $M_r < -20$). Both models assume $h = 0.7$ and $\sigma_8 = 0.8$. The w_{gg} model fitted for the $17 < r < 21$ galaxies is $w_{gg}(\theta) = 0.142\theta^{-0.70}$ (red, long dashes). (b) The cross-correlation function, $w_{gq}(\theta)$, for $17 < g < 19$ QSO candidates and $17 < r < 21$ galaxies, compared to the two HOD models and the two models of Williams & Irwin (1998) with $b = 1.25$ and $b = 0.75$. (c) The same as (b) for the $20 < g < 21$ limited QSO case.

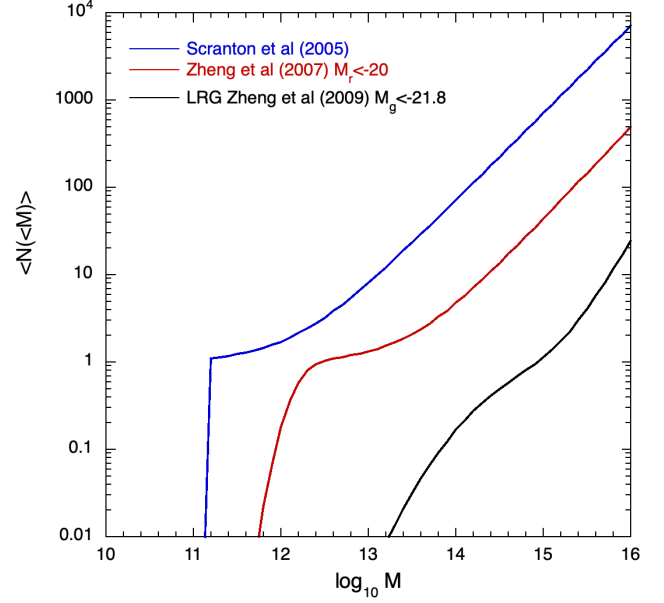


Figure 8. HOD models of Scranton et al (2005) (with $\log(M_{\min}) = 11.15(11.0)$, $\sigma_M = 0.01$, $\log(M_0) = 0.0$, $\log(M'_1) = 12.15(12.0)$, $\alpha = 1.0$) and Zheng et al (2007) $M_r < -20$ model (with $\log(M_{\min}) = 12.17(12.02)$, $\sigma_M = 0.26$, $\log(M_0) = 11.53(11.38)$, $\log(M'_1) = 13.46(13.31)$, $\alpha = 1.06$). The LRG model is from Zheng et al (2009) (with $\log(M_{\min}) = 14.45(14.30)$, $\sigma_M = 0.71$, $\log(M_0) = 12.64(12.49)$, $\log(M'_1) = 15.10(14.95)$, $\alpha = 1.35$). All masses assume $h = 0.7$ ($h = 1$).

In searching for an improved HOD model, we then considered the HOD recommended for SDSS galaxies with $M_r < -20$ by Zheng et al. (2007) as an alternative to the simple S05 HOD. The parameters of this model are given in the caption of Fig. 8. This model produces slightly improved agreement with the ATLAS w_{gg} at both small and large scales. We also considered the range of HOD models fitted to SDSS semi-projected correlation functions $w_p(\sigma)$ by Zehavi et al. (2011) (see their Fig. 10 and Table 3) corresponding to galaxies with absolute magnitudes from $M_r < -18.0$ to $M_r < -22.0$ but no better fit to our $17 < r < 21$ w_{gg} was found.

In more general searches within the 5-parameter HOD scheme of Zheng et al. (2007), we still found it difficult to improve on the above SDSS $M_r < -20$ HOD as a description of the ATLAS w_{gg} . Given the excellent agreement of the ATLAS w_{gg} and the SDSS w_{gg} of Wang et al. (2013), also shown in Fig. 7a, we have no reason to believe that this HOD fitting issue stems from the ATLAS data. So, bearing in mind these residuals at small and large scales, we shall consider the above two HOD models as reasonable fits and proceed to test them further using our weak lensing analyses.⁶

5.2 HOD modelling from galaxy-quasar lensing

We then continue to follow the method of Jain et al. (2003) to predict the w_{gk} cross-correlations, first assuming the Scranton et al. (2005) HOD. Having multiplied the model w_{gk} 's in Fig. 7(a) by $(2.5\alpha - 1) = 0.95, -0.37$ for the bright $17 < g < 19$ and faint $20 < g < 21$ QSO samples, we compare the Scranton et al. (2005)

⁶ Fitting a -0.8 power law to our w_{gg} at $\theta < 60'$ and then applying Limber's formula gives a 3-D correlation function scale-length of $r_0 = 5h^{-1}$ Mpc.

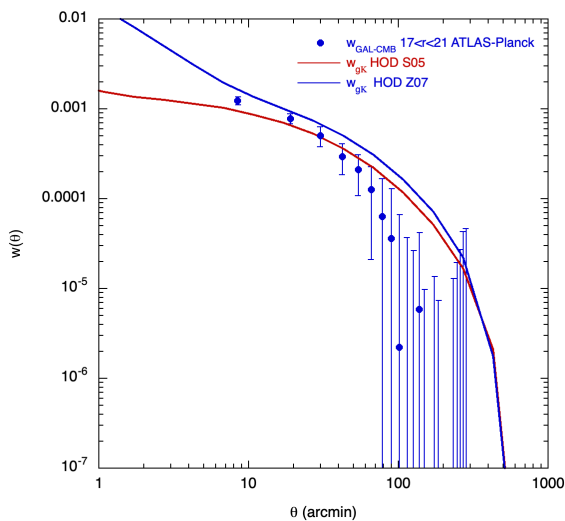


Figure 9. w_{g-CMB} cross-correlation function for $17 < r < 21$ galaxies and the Planck (2018) Lensing Map with field-field errors, compared to the HOD models of Scranton et al. (2005) and Zheng et al. (2007) (with $M_r < -20$). Both models assume $h = 0.7$ and $\sigma_8 = 0.8$. The first bin centre at $6'$ corresponds to $\approx 1 \text{ h}^{-1}\text{Mpc}$ at the galaxy mean z of $z = 0.15$.

and Zheng & Weinberg (2007) HOD predictions to our w_{gq} results in Figs. 7(b, c). In turn, we compare these to the $w_{gm} = w_{gg} \times 2\bar{\kappa}/b$ Williams & Irwin (1998) models with $b = 0.5$ and $b = 1.25$. The Zheng et al. (2007) HOD model seems to give a better fit than the Scranton et al. (2005) model in Figs. 7(b, c), with both models fitting these data better than the standard $b = 1.25$ ($\sigma_8 = 0.8$) Williams & Irwin (1998) model. Indeed, in Figs. 7(b, c) we see that the HOD model of Zheng et al. (2007) gives almost as good a fit as the best fit, $b = 0.5$, Williams & Irwin (1998) model. However, the errors are still large in Figs. 7(b, c) and we remain wary about the size of the small-scale ($\theta < 0.5'$) anti-correlation of the stellar control sample in Fig. 7(c). Another issue is that looking back at Fig. 7(a) we note that, at $\theta > 1'$, the predicted w_{gk} for the two HOD models with $\sigma_8 = 0.8$ lies significantly below the best fit, $b = 0.5$ (or $\sigma_8 = 2$), Williams & Irwin (1998) model implying that both sets of models cannot fit the data equally well on these larger scales. This motivates a more detailed study of the 1-halo term using LRGs in Section 6 below, while a further test of the 2-halo fit of the HOD models is available from the CMB lensing test in Section 5.3 below. However, our main conclusion at this point is that we confirm that HOD models can be found that simultaneously give reasonable fits to w_{gg} and w_{gq} at small scales and that these fit w_{gq} significantly better than simpler models that assume galaxies trace the mass with bias in the standard ΛCDM $b \approx 1.2 - 1.4$ (or $\sigma_8 \approx 0.7 - 0.8$) range.

5.3 Further Galaxy-CMB lensing test of HOD models

In Fig. 9 we show the $17 < r < 21$ galaxy - Planck CMB Lensing Map cross-correlation function compared to the predictions of the HOD models of Scranton et al. (2005) and Zheng et al. (2007). Here we see that the data is in reasonable agreement with the Scranton et al. (2005) model at all scales (with a reduced χ^2 of 2.67) and fits particularly well in the range $10' < \theta < 60'$ with a reduced χ^2 of 1.15, whereas the Zheng et al. (2007) model appears to over-predict the data at all scales (with a reduced $\chi^2 > 10$), despite its good fit to w_{gg} at $\theta > 20'$. We also note that the scales probed with the Planck map are mostly at the scales of the 2-halo term with $r_{com} \approx 1 \text{ h}^{-1}$

Mpc corresponding to $\theta \approx 8'$ at the average galaxy redshift of $z = 0.15$. So CMB lensing at Planck resolution is clearly the test of choice for the 2-halo term while the galaxy QSO cross-correlation function in Fig. 7 (b),(c), with its scale extending down to $\approx 1'$, provides a better test of the 1 halo-term. Here we have seen that both S05 and Z07 models give reasonable fits to w_{gq} but the S05 HOD fits the CMB lensing data better than the Z07 HOD galaxy at larger scales, despite both HOD models fitting the w_{gg} equally well in this range dominated by the 2-halo term. But higher signal-noise data for QSO lensing and higher resolution data for CMB lensing should give further interesting tests of both the 1- and 2-halo terms of these galaxy halo occupation models independently over the full range of scales.

6 LRG HOD MODELLING

We next attempt to model the VST ATLAS LRG sample that are assumed to occupy the $0.16 < z < 0.36$ range with an approximately flat $n(z)$ (see Fig. 12 of Eisenstein et al. 2001). From Fig. 10 (a) we see that the LRG auto-correlation function $w_{LRG-LRG}$ is $\approx 10\times$ higher than the $17 < r < 21$ galaxy w_{gg} in Fig. 7 (a). The higher amplitude clustering of the LRGs will allow more powerful weak lensing tests of the 1- and 2-halo terms for HODs claimed to be appropriate for LRGs. So we shall now test the LRG HOD model advocated by Zheng et al. (2009) with $M_g < -21.8$ (see Fig. 8) and first compare it to our LRG $w_{gg}(\theta)$ in Fig. 10 (a). While reaching the amplitude of the observed LRG $w_{gg}(\theta)$ at $\theta \approx 1'$, we see that the HOD predicted w_{gg} again underestimates the observations at scales of $\approx 10'$, similar to what was found for the $17 < r < 21$ galaxy HOD model of Zheng et al. (2007) in Fig. 7 (a). The fit also appears somewhat worse at large scales than found for the SDSS LRG $w_p(\sigma)$ by Zheng et al. (2009). Nevertheless, since the HOD model fits w_{gg} in the range $\theta < 5'$ we again suggest that it is a useful basis to test the HOD model of Zheng et al. (2009) against the simpler Williams & Irwin (1998) model using the LRG-QSO cross-correlations as considered in Section 6.1 below.

6.1 LRG-QSO lensing

As before for galaxies, we investigate the mass distribution around LRGs by analysing their cross-correlation with $17 < g < 19$ and $20 < g < 21$ ATLAS QSO samples, but based here first on the Zheng et al. (2009) HOD model for w_{gk} as shown by the dashed line in Fig. 10 (a). We see that for the $20 < g < 21$ QSO case in Fig. 10 (c), a significant anti-correlation signal is seen at $\theta < 5'$ and particularly at $\theta \approx 0.3'$ where $w_{gq} \approx -0.17$, even taking into account that the control star sample also shows a less significant anti-correlation at $\theta \approx 0.3'$. However, a less strong signal is seen in the $17 < g < 19$ case in Fig. 10 (b) where w_{gq} is consistent with zero at all scales; we note that the errors are larger here. We then checked for the presence of dust by re-doing the cross-correlations with the QSO samples limited at bright and faint W1 magnitudes. The bright cross-correlation is expected to increase more than the faint cross-correlation in the case of dust due to the steeper QSO $n(g)$. However, both the bright and faint W1 cross-correlations were consistent with the g-limited results in Figs. 10 (b, c). Inspection of the w_{gq} results in the 8 sub-areas used for the field-field errors also showed that the anti-correlation existed in almost all sub-areas.

We compare to the model of Zheng et al. (2009) for

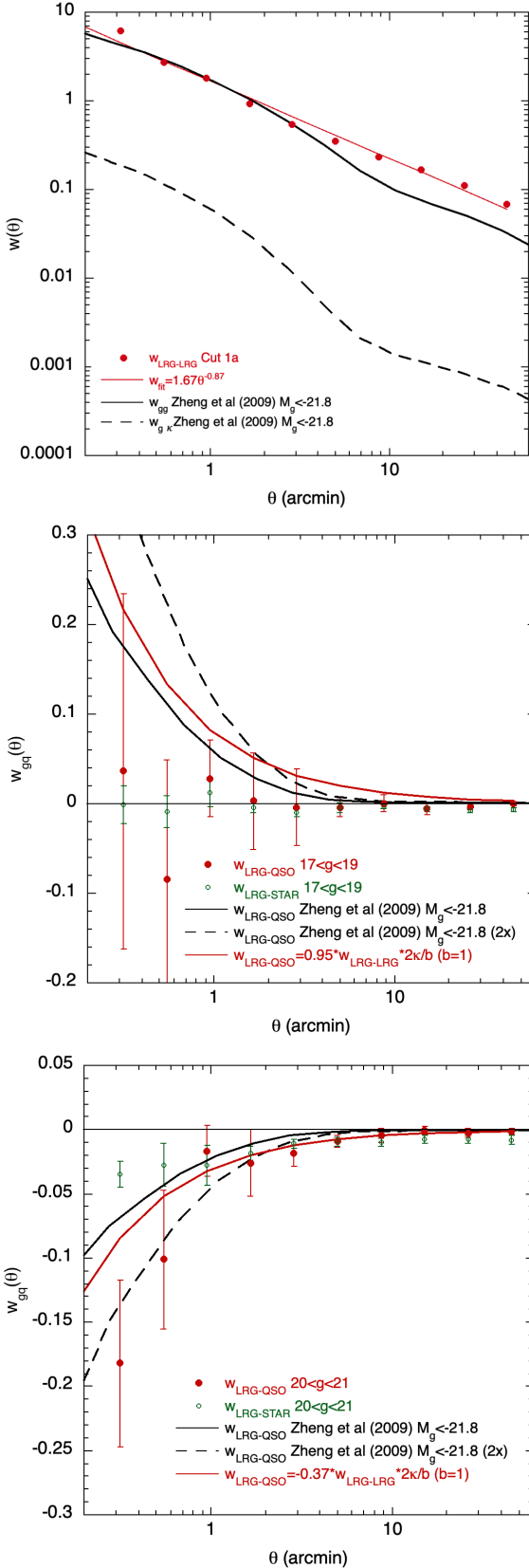


Figure 10. (a) w_{gg} and w_{gk} auto- and cross-correlation functions predicted by the HOD model of Zheng et al. (2009) for $M_g < -21.8$ SDSS LRGs (with $\sigma_8 = 0.8$ and $h = 0.7$), compared to $w_{gg}(\theta)$ for our LRGs. (b) The cross-correlation function, $w_{gq}(\theta)$, for $17 < g < 19$ QSO's and our LRG sample, compared to the HOD model of Zheng et al. (2009) and the 2 models of Williams & Irwin (1998) with $b = 1$ and $b = 0.6$. (c) Same as (b) for the QSO magnitude range $20 < g < 21$.

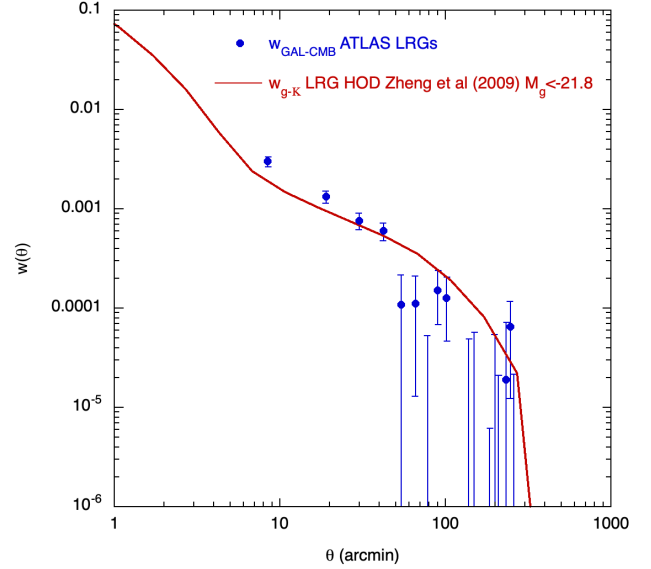


Figure 11. w_{g-CMB} cross-correlation function for our LRG sample with $0.16 < z < 0.36$ and the Planck (2018) Lensing Map with field-field errors, compared to the HOD model of Zheng et al. (2009) with parameters $\log(M_{\text{min}}) = 14.45$, $\sigma_M = 0.80$, $\log(M_0) = 12.64$, $\log(M_1) = 15.10$, $\alpha = 1.72$. The model assumes $h = 0.7$ and $\sigma_8 = 0.8$. The first bin centre at $6'$ corresponds to $\approx 1 h^{-1}\text{Mpc}$ at the LRG mean z of $z = 0.26$.

$M_g < -21.8$ LRG's (solid black line) and see that although it is consistent with the bright QSO cross-correlation in Fig. 10 (b), it remains above the less noisy faint QSO result at most scales below $\theta \approx 5'$ in Fig. 10 (c), although the reduced χ^2 is still only 1.73 for these 6 points. As in Section 6 above, we have assumed a flat $n(z)$ in the range $0.16 < z < 0.36$ for the LRGs, following Eisenstein et al. (2001). A Williams & Irwin (1998) model with $b = 1$ based on the LRG-LRG autocorrelation function in Fig. 10 (a) is also shown in Figs. 10 (b, c) assuming the same optical depth ($\kappa = 0.025$) used previously for the $r < 21$ galaxy sample in Section 4. This model assumes that the LRGs trace the mass and this model does get closer to the w_{gq} results than the above HOD model. However, the low point at $\theta = 0.3$ remains over-estimated by both. To check if it's the form or the amplitude of the halo mass profile that is causing the problem we show the HOD model multiplied by a factor of 2 as the dashed line in Fig. 10 (c); the fit improves suggesting that it may be the amplitude rather than the form of the NFW mass profile that is at fault.

We conclude that the Zheng et al. (2009) LRG HOD that gives a reasonable fit to the ATLAS LRG w_{gg} at least at small, $\theta < 2'$ scales may be rejected by w_{gq} in the same angular range. The problem seems to be that the effective bias produced by the HOD appears too small and a higher amplitude mass profile may be needed to improve the fit. We also note that the LRG HOD also underestimates the LRG w_{gg} at larger scales and this might only be addressed by using a higher value of $\sigma_8 > \approx 1$ which seems another problem for the LRG HOD approach at larger scales to put alongside the lensing magnification problem at smaller scales.

6.2 Further LRG-CMB lensing test of HOD model

In Fig. 11 we show the $0.16 < z < 0.36$ LRG cross-correlation with the Planck CMB lensing convergence map compared to the prediction of the Zheng et al. (2009) HOD model. Overall, the model fits the data well, giving reduced $\chi^2 = 1.7$. Looking in more detail and in the context of the fit of the Z09 model to the LRG w_{gg} in Fig. 10(a), we see reasonable agreement between the data and model here for the 2-halo term at $\theta > 10'$ although this is the range where the model significantly underpredicts the LRG w_{gg} . At smaller scales where the Z09 model fits the LRG w_{gg} very well, the CMB lensing prediction is too low compared to the observed result, in agreement with the LRG-QSO cross-correlation result seen in Fig. 10(c). Thus the LRG HOD model either fits the LRG w_{gg} while underestimating the QSO and CMB lensing results at small scales or underpredicts the LRG w_{gg} while fitting the CMB lensing result at large scales. This is reasonably consistent with the galaxy lensing results in Section 5.3, where at small scales the HOD underestimates the galaxy-QSO cross-correlation w_{gq} relative to the galaxy w_{gg} whereas at large scales the Z07 HOD, at least, fits w_{gg} while over-predicting the galaxy CMB lensing result. However, the LRG results are stronger because of their high amplitude and signal-noise. Similar large scale behaviour may also be seen in the CMB lensing results for the $n > 5$ groups and clusters sample in Fig. 4 and Table 1 of Section 3.5.

7 CONCLUSIONS

We have detected lensing magnification of background quasars by foreground clusters, galaxies and LRGs. We have used stars as control samples and these have suggested there may be a sky-subtraction problem for the NEO7 and DECALS DR10 W1 and W2 magnitudes when measured in the vicinity of bright galaxies. We have also investigated lensing of the CMB by these VST ATLAS cluster and galaxy samples and detected strong effects in each case.

From the lensing of ATLAS quasars by galaxy clusters in the ATLAS catalogue of Ansarinejad et al. (2023) we find that NFW profiles with halo masses of $\approx 1 \times 10^{15} M_{\odot}$ fit clusters with $n > 40$ members with $\approx 1 \times 10^{14} M_{\odot}$ fitting groups/clusters of $n > 5$ members. The $n > 40$ clusters show the greatest signal but both cluster samples show a preference for an NFW profile over an SIS at the small scales probed by quasar lensing. The larger scales dominated by the 2-halo terms are much better investigated using CMB lensing. Cross-correlation of the Planck CMB lensing convergence map with the galaxy clusters showed very strong signals for both cluster samples and we find cluster masses of $\approx 1 \times 10^{14} M_{\odot}$ for the $n > 5$ clusters and $\approx 3 \times 10^{14} M_{\odot}$ for the $n > 40$ clusters. Overall, the quasar and CMB lensing mass estimates are in good agreement for both samples. However, the CMB lensing cross-correlation is less well fitted by the $n > 5$ sample than is the $n > 40$ sample. Also while the quasar and CMB lensing masses bracket the average masses quoted for the $n > 40$ clusters, the lensing mass estimates for the $n > 5$ sample are generally lower than those quoted by Ansarinejad et al. (2023) by a factor of $\approx 3 - 5$.

For the VST ATLAS $17 < r < 21$ galaxy sample, we find that galaxy-galaxy angular auto-correlation and the quasar - galaxy cross-correlation results are consistent with those for SDSS galaxies by respectively Wang et al. (2013) and Scranton et al. (2005) and both are at similar levels of significance. We then addressed the question of how e.g. Myers et al. (2005) found too high a level of QSO magnification for compatibility with standard Λ CDM cosmology compared to Scranton et al. (2005) who found that the SDSS

QSO magnification studies were consistent with standard cosmology predictions. Generally we agree with the previous conclusions of Mountrichas & Shanks (2007) that the actual observations are very consistent with each other and that the difference lay in the models used to interpret these quasar-galaxy cross-correlations. Previously, Myers et al. (2005) assumed that galaxies traced the mass up to a linear bias factor and we have again shown on this assumption that values of the galaxy bias much smaller than unity or equivalently values of σ_8 higher than unity are needed for such models to fit. If instead the HOD approach of Scranton et al. (2005) is followed, then models such as the SDSS $M_r < -20.8$ model of Zheng & Weinberg (2007) can be found that at least approximately fit our measured galaxy angular auto-correlation function while simultaneously reasonably fitting the QSO-galaxy cross-correlation function at the same scales. However, there is a hint that the Zheng & Weinberg (2007) model that fits w_{gg} is still slightly too low in lensing magnification amplitude at the smallest scales of w_{gq} . Our strong detection of the ATLAS galaxy- Planck CMB lensing signal was also slightly over-predicted by the Zheng & Weinberg (2007) HOD model at a similar level as the 2-halo term's over-prediction of the group/cluster $n > 5$ sample. But both these deficiencies were only marginally detected and this motivated us to look at the lensing results for the more extreme case of highly clustered LRGs to see if any such problems persisted there.

We therefore selected a sample of ATLAS $r < 19.5$ LRG's, using similar criteria to the SDSS Cut 1 of Eisenstein et al. (2001) with a $0.16 < z < 0.36$ redshift range and found an LRG auto-correlation function amplitude $\approx 10\times$ that of the above $17 < r < 21$ galaxy sample. We found that the LRG HOD of Zheng et al. (2009) again fitted $w_{gg}(\theta)$ well at small scales but underestimated w_{gg} at larger scales, similar to the galaxy HOD. We then compared the LRG HOD prediction to the QSO-LRG cross-correlation function and found that it under-predicted the amplitude of the LRG anti-correlation with $20 < g < 21$ ATLAS quasars, at a level stronger than the hint in the $17 < r < 21$ galaxy w_{gq} . Multiplying the LRG HOD prediction by a factor of 2 significantly improved the fit, demonstrating the size of the effect. The $17 < g < 19$ QSO-LRG cross-correlation showed less discrepancy with the HOD prediction but here the errors are much larger.

Overall, we conclude that our QSO-galaxy cross-correlation results are in good agreement with previous authors for clusters and $17 < r < 21$ galaxies and that HOD models improve standard Λ CDM cosmology fits, in particular in the $17 < r < 21$ galaxy case compared to models where galaxies trace the mass. In the case of clusters, NFW mass profiles are preferred over SIS profiles, with NFW mass estimates compatible with previous results for both clusters and groups. CMB lensing results for groups tended to be under-predicted by standard 2-halo models and this was also seen marginally in the CMB lensing of the $17 < r < 21$ galaxies. LRGs show the biggest discrepancies with a standard HOD model, where they under-predict w_{gq} by a factor of $\approx 2\times$ in the fainter QSO samples, while over-predicting the LRG-CMB lensing result by a smaller factor. Further investigation is required to see if improved HOD models can be found to address these anomalies at large and small scales in the galaxy, group and particularly LRG samples.

DATA AVAILABILITY STATEMENT

The ESO VST ATLAS and WISE data we have used are all publicly available. The VST ATLAS QSO Catalogue can be found at https://astro.dur.ac.uk/cea/vstatlas/qso_

catalogue/. All other data relevant to this publication will be supplied on request to the authors.

ACKNOWLEDGEMENTS

We acknowledge use of the ESO VLT Survey Telescope (VST) ATLAS. The ATLAS survey is based on data products from observations made with ESO Telescopes at the La Silla Paranal Observatory under program ID 177.A-3011(A,B,C,D,E,F,G,H,I,J,K,L,M,N) (see Shanks et al. 2015).

We acknowledge the use of data products from WISE, which is a joint project of the University of California, Los Angeles, and the Jet Propulsion Laboratory (JPL)/California Institute of Technology (Caltech), funded by the National Aeronautics and Space Administration (NASA), and from NEOWISE, which is a JPL/Caltech project funded by NASA.

We acknowledge use of SDSS imaging and spectroscopic data. Funding for SDSS-III has been provided by the Alfred P. Sloan Foundation, the Participating Institutions, the National Science Foundation and the US Department of Energy Office of Science.

BA acknowledges support from the Australian Research Council's Discovery Projects scheme (DP200101068).

LFB acknowledges support from ANID BASAL project FB210003.

We finally acknowledge STFC Consolidated Grant ST/T000244/1 in supporting this research.

For the purpose of open access, the author has applied a Creative Commons Attribution (CC BY) licence to any Author Accepted Manuscript version arising.

We thank the referee for useful comments that have improved the paper.

REFERENCES

- Alonso D., 2012, arXiv e-prints, [p. arXiv:1210.1833](https://arxiv.org/abs/1210.1833)
- Ansarinejad B., Murphy D., Shanks T., Metcalfe N., 2023, *MNRAS*, **520**, 1371
- Blanchard A., Schneider J., 1987, *A&A*, **184**, 1
- Boyle B. J., Fong R., Shanks T., 1988, *MNRAS*, **231**, 897
- Bullock J. S., Kolatt T. S., Sigad Y., Somerville R. S., Kravtsov A. V., Klypin A. A., Primack J. R., Dekel A., 2001, *MNRAS*, **321**, 559
- Croom S. M., 1997, PhD thesis, -
- Croom S. M., et al., 2005, *MNRAS*, **356**, 415
- Eisenstein D. J., et al., 2001, *AJ*, **122**, 2267
- Eltvedt A. M., et al., 2023, *MNRAS*, **521**, 3384
- Geach J. E., Peacock J. A., Myers A. D., Hickox R. C., Burchard M. C., Jones M. L., 2019, *ApJ*, **874**, 85
- Han J., Ferraro S., Giusarma E., Ho S., 2019, *MNRAS*, **485**, 1720
- Heymans C., et al., 2021, *A&A*, **646**, A140
- Jain B., Scranton R., Sheth R. K., 2003, *MNRAS*, **345**, 62
- Kaiser N., 1998, *ApJ*, **498**, 26
- Kaiser N., Squires G., 1993, *ApJ*, **404**, 441
- Krolewski A., Ferraro S., Schlafly E. F., White M., 2020, *J. Cosmology Astropart. Phys.*, **2020**, 047
- Krolewski A., Ferraro S., White M., 2021, *J. Cosmology Astropart. Phys.*, **2021**, 028
- Kron R. G., 1980, *ApJS*, **43**, 305
- Limber D. N., 1953, *ApJ*, **117**, 134
- Mead A. J., Verde L., 2021, *MNRAS*, **503**, 3095
- Ménard B., Scranton R., Fukugita M., Richards G., 2010, *MNRAS*, **405**, 1025
- Ménard B., Wild V., Nestor D., Quider A., Zibetti S., Rao S., Turnshek D., 2011, *MNRAS*, **417**, 801

- Metcalfe N., Shanks T., Fong R., Jones L. R., 1991, *MNRAS*, **249**, 498
- Mountrichas G., Shanks T., 2007, *MNRAS*, **380**, 113
- Mountrichas G., Sawangwit U., Shanks T., Croom S. M., Schneider D. P., Myers A. D., Pimblet K., 2009, *MNRAS*, **394**, 2050
- Murphy D. N. A., Geach J. E., Bower R. G., 2012, *MNRAS*, **420**, 1861
- Myers A. D., Outram P. J., Shanks T., Boyle B. J., Croom S. M., Loaring N. S., Miller L., Smith R. J., 2003, *MNRAS*, **342**, 467
- Myers A. D., Outram P. J., Shanks T., Boyle B. J., Croom S. M., Loaring N. S., Miller L., Smith R. J., 2005, *MNRAS*, **359**, 741
- Narayan R., 1989, *ApJ*, **339**, L53
- Narayan R., Nityananda R., 1985, in Kapahi V. K., ed., *Extragalactic Energetic Sources*. p. 149
- Navarro J. F., Frenk C. S., White S. D. M., 1996, *ApJ*, **462**, 563
- Peebles P. J. E., 1974, *ApJ*, **189**, L51
- Peebles P. J. E., 1980, *The large-scale structure of the universe*. Princeton University Press
- Perlmutter S., et al., 1999, *ApJ*, **517**, 565
- Petter G. C., et al., 2022, *ApJ*, **927**, 16
- Petter G. C., Hickox R. C., Alexander D. M., Myers A. D., Geach J. E., Whalen K. E., Andonie C. P., 2023, *ApJ*, **946**, 27
- Planck Collaboration et al., 2018, arXiv e-prints, [p. arXiv:1807.06210](https://arxiv.org/abs/1807.06210)
- Planck Collaboration et al., 2020, *A&A*, **641**, A6
- Ratra B., Peebles P. J. E., 1988, *Phys. Rev. D*, **37**, 3406
- Riess A. G., et al., 1998, *AJ*, **116**, 1009
- Rubin V. C., Thonnard N., Ford W. K. J., 1977, *ApJ*, **217**, L1
- Schlafly E. F., Meisner A. M., Green G. M., 2019, *ApJS*, **240**, 30
- Scranton R., et al., 2005, *ApJ*, **633**, 589
- Seldner M., Peebles P. J. E., 1979, *ApJ*, **227**, 30
- Seljak U., 1996, *ApJ*, **463**, 1
- Shanks T., et al., 2015, *MNRAS*, **451**, 4238
- Wang Y., Brunner R. J., Dolence J. C., 2013, *MNRAS*, **432**, 1961
- Williams L. L. R., Irwin M., 1998, *MNRAS*, **298**, 378
- Zehavi I., et al., 2011, *ApJ*, **736**, 59
- Zheng Z., Weinberg D. H., 2007, *ApJ*, **659**, 1
- Zheng Z., Coil A. L., Zehavi I., 2007, *ApJ*, **667**, 760
- Zheng Z., Zehavi I., Eisenstein D. J., Weinberg D. H., Jing Y. P., 2009, *ApJ*, **707**, 554
- Zwicky F., 1933, *Helvetica Physica Acta*, **6**, 110

This paper has been typeset from a $\text{\TeX}/\text{\LaTeX}$ file prepared by the author.